COMPUTATIONAL MODELLING OF SQUAT AND RESISTANCE OPTIMISATION IN FULLY CONFINED WATER

Momchil Terziev - Department of Naval Architecture, Ocean and Marine Engineering, University of Strathclyde, Glasgow, UK
Muhammad Iqbal - Department of Naval Architecture, Faculty of Engineering, Universitas Diponegoro, Indonesia
Yujia Wei - School of Aerospace, Transport and Manufacturing, University of Cranfield, UKAtilla Incecik - Department of Naval Architecture, Ocean and Marine Engineering, University of Strathclyde, Glasgow, UK

COMPUTATIONAL MODELLING OF SQUAT AND RESISTANCE OPTIMISATION IN FULLY CONFINED WATER

MOMCHIL TERZIEV - DEPARTMENT OF NAVAL ARCHITECTURE, OCEAN AND MARINE ENGINEERING, UNIVERSITY OF STRATHCLYDE, GLASGOW, UK.
MUHAMMAD IQBAL - DEPARTMENT OF NAVAL ARCHITECTURE, FACULTY OF ENGINEERING, UNIVERSITAS DIPONEGORO, INDONESIA.
YUJIA WEI - SCHOOL OF AEROSPACE, TRANSPORT AND MANUFACTURING, UNIVERSITY OF CRANFIELD, UK.
ATILLA INCECIK - DEPARTMENT OF NAVAL ARCHITECTURE, OCEAN AND MARINE ENGINEERING, UNIVERSITY OF STRATH-CLYDE, GLASGOW, UK.

SUMMARY

Ship squat in confined waters is of critical importance for safe and efficient operations. However, little is known about the relationship between the magnitude of the maximum squat and the resistance, and if it is possible to reduce squat by imposing changes in trim through variations in the position of the centre of gravity of a ship. The present paper investigates these questions through the use of Reynolds Averaged Navier-Stokes modelling, applied to the KRISO container ship at a scale of 1:75. It is found that at the low speed investigated of F_h =0.303, the dynamic trim is dominated by the initial assignment and changes in sinkage are responsible for a complex behaviour exhibited by the total resistance. The set of optimum values expressing the trade-off between squat and resistance is found to be such that higher squat values are predicted to be able to improve resistance at the investigated speed.

NOMENCLATURE

B	Ship beam (m)
C_F	Frictional resistance coefficient (-)
CFD	Computational Fluid Dynamics
C_M	Midship section coefficient (-)
C_P	Pressure resistance coefficient (-)
C_T	Total resistance coefficient (-)
dy	Wall-normal distance to first cell centre (m)
F_h	Depth Froude number = $V/\sqrt{gh}$ (-)
h	Canal depth (m)
h/T	Depth-to-draft ratio (-)
L	Ship length (m)
LC	Loading condition (-)
p	Observed order of accuracy = $\log(\varepsilon_{21}/\varepsilon_{32})$ /log (r) (-)
R	Convergence ratio= $\varepsilon_{32}/\varepsilon_{21}$ (-)
r	Refinement factor = $\sqrt{2}$ (-)
S	Common ratio in geometric series expressing the distribution of near-wall layers (-)
s	Ship sinkage (m)
S_w	Wetted surface area
T	Ship draft (m)
U	Discretisation uncertainty (%)
U_E	Experimental uncertainty (%)
U_N	Numerical uncertainty (%)
U_V	Validation uncertainty (%)
w/L	Width to length ratio (-)
y^+	Dimensionless wall-normal distance (-)
B_R	Blockage ratio

δ	Boundary layer thickness $= 0.382L/Re^{1/5}$ (m)
ε	Difference between the coarse and medium solutions (ε_{32}) and medium and fine solutions (ε_{21}).
θ	Ship trim (°)
λ	Scale factor (-)
μ	Dynamic viscosity (Pa-s)
ν	Kinematic viscosity (m^2/s)
ρ	Density of water (kg/m^3)
τ_w	Shear wall stress (Pa)

1 INTRODUCTION

Much attention has been paid to trim optimisation as a rational and low-cost approach to reduce the power requirements of a vessel sailing in calm water. However, the dynamic attitude of a hull is influenced by the fore-aft imbalance in forces and moments while underway, modifying the running trim and sinkage from the condition assigned at rest. Such effects are small in unrestricted waters, but may pose a threat of grounding in shallow and laterally restricted waterways. Therefore, one may ask if it is possible to cancel squat-induced trim by modifications to the loading condition, for example by moving ballast water within the hull. It is widely believed that such modifications can only magnify squat, but Härting et al. (2009) questioned the validity such assertions and demonstrated that it may be possible to reduce overall squat. Alternatively, it may be asked what the relationship between an optimum squat and resistance is.

Unlike deep water performance, to the best of the authors' knowledge, confined water performance through the lens of trim optimisation has received little attention since the work of Härting et al. (2009). In the field of trim optimisaiton, many researchers have recently opted to use statistical and AI type models which typically employ full-scale data (Cisek, 2025; Panagiotakopoulos et al., 2022; Tu et al., 2023). Regrettably, the necessary datasets are usually proprietary and to the best of the authors' knowledge, there exist no openly available full-scale datasets, including the ship geometry where confined and shallow water performance is concerned. Since each ship's performance, and therefore, dynamic attitude while underway, are unique, models built on proprietary data featuring a single hull or a limited number of hulls cannot yet replace the need for deterministic models, an overview of which was recently given by Korkmaz et al. (2023). A widely used alternative in practice due to the speed of the prediction are empirical methods, summarized by Barrass & Derrett (2012). However, empirical models are simplistic and tend to significantly overestimate squat. While that ought to mean fewer groundings, data from the European Maritime Safety Agency data consistently shows that groundings are in the top accident categories and that the majority of accidents occur in shallow water (EMSA (European Maritime Safety Agency), 2023).

The present paper uses Computational Fluid Dynamics (CFD) to assess the possibility of simultaneously negating changes dynamic in trim and reducing resistance through modifications of the static trim by modifying the loading condition of a ship. CFD has the advantage of solving the viscous effect which is likely of considerable importance in very shallow and narrow conditions. Viscous effects have been recently shown to be of critical importance in the calculation of the trim, first by Chillcce & Moctar (2022) who modelled various approaches of accounting for the viscous term in computational squat modelling and more recently by Le Strat & Terziev (2025) who investigated the scale effect acting on the force causing sinkage and trim finding that the trim moment exhibits sensitivity to the Reynolds number, and therefore, viscosity.

The approach taken herein is to employ the response surface methodology requiring a set of 9 results to produce the optimum. Each of the 9 data points for squat and resistance, respectively, are obtained using the commercially available Navier-Stokes solver Star-CCM+, and which are used to construct a Pareto front showing the trade-offs between squat and resistance. This study proceeds with a laying out of the employed case studies and validation condition, followed by the numerical model and details of the computational mesh. Results and discussion are preceded by a brief overview of the optimisation procedure. Finally, conclusions and recommendations for future work are given.

2 CASE STUDIES

To maximise the reproducibility of the subsequently presented results, the KRISO Container Ship (KCS) in model scale of 1:75 is used throughout. The scale factor is chosen to match that experimented upon by Elsherbiny et al. (2019), whose study included a rectangular canal of dimensions shown in Table 1.

Table 1. Ship principal dimensions and basis bathymetry geometry

Parameter	Symbol	Full-scale	Model-scale	Units
Scale factor	λ	1	75	-
Ship length	L	230	3.067	m
Beam	B	23.2	0.429	m
Draft	T	10.8	0.144	m

Midship area coefficient	C_M	0.985	0.985	-
Depth-to-draft ratio	h/T	2.22	2.22	-
Width-to-length ratio	w/L	1.5	1.5	-
Depth Froude number	F_h	0.303	0.303	-

The conditions given in Table 1 are used for validation to ensure the numerical model has sufficient accuracy against a basis condition, which is subsequently modified to explore the effects of depth and width on the resulting optima. Once the above condition is validated following the ITTC (2008) procedure, a set of alterations are imposed on the canal geometry to gauge the sensitivity of the optimum loading condition on the length and width of the waterway. The full description of the loading conditions and canal geometry variations are given in Table 2.
The loading conditions given in Table 2 are replicated for each of the canal geometry condition. The values moment of inertia result from the difference in the position of the centre of gravity, measured from the aft perpendicular of the ship and varied within ±2.5% of the initial condition in the horizontal and ±5% in the vertical direction.

Table 2. Investigated loading conditions and canal geometries. LC stands for loading condition; the initial condition is labelled 0. The vase studies were obtained using a systematic variation determined by the optimisation procedure

LC	Parameter										
	LCG (m)	KG (m)	Rx (m)	Ry (m)	Rz (m)	I_{xx} (kgm^2)	I_{yy} (kgm^2)	I_{zz} (kgm^2)	h/T	w/L	F_h
0*	1.487	0.149	0.134	0.791	0.796	1.099	38.408	38.851	2.22, 2, 1.8	1.5, 1	0.303
1	1.524	0.156	0.135	0.791	0.795	1.111	38.369	38.801			
2	1.524	0.142	0.135	0.791	0.795	1.093	38.351	38.801			
3	1.450	0.156	0.135	0.794	0.798	1.111	38.638	39.070			
4	1.450	0.142	0.135	0.793	0.798	1.093	38.621	39.070			
5	1.434	0.149	0.135	0.795	0.800	1.099	38.773	39.217			
6	1.540	0.149	0.135	0.791	0.796	1.099	38.387	38.831			
7	1.487	0.138	0.133	0.791	0.796	1.092	38.401	38.851			
8	1.487	0.160	0.135	0.791	0.796	1.120	38.429	38.851			

*Condition used for validation

3 NUMERICAL MODEL

All results are obtained using the commercially available Navier-Stokes solver, Star-CCM+, version 18.02.010. The set up explained herein is replicated across case studies and intended to maximise reproducibility of the results.
The solver makes use of the Finite Volume method to discretise the computational domain into a finite number of adjoining cells. For the purposes of the present paper, the Reynolds Averaged Navier-Stokes approach was used throughout with the standard *k*-ω turbulence model following the recommendations of Terziev et al. (2019). Second order discretisation was used for all parameters except time marching where a first order scheme was used to improve stability and relax the conditions of the Courant number on the free surface. The value of the time step was selected by $\Delta t = 0.0035V/L$ following Terziev et al. (2018). Multiphase flow was modelled in all cases where the air-water interface is resolved using the Volume of Fluid method (Hirt & Nichols, 1981).

3.1 COMPUTATIONAL DOMAIN AND BOUNDARY CONDITIONS

The computational domain consisted of a rectangular box with a global coordinate system coincident with the ship aft perpendicular. Half of the problem was modelled to reduce the number of required cells. The boundary bisecting the ship was assigned a symmetry plane boundary condition, the domain bottom and side were no-slip walls placed according to the conditions given in Table 1, and assigned a tangential velocity equal and opposite that of the ship's. The ship geometry was set as a no-slip wall, while the upstream boundary was assigned a velocity inlet condition and the downstream boundary - a pressure outlet condition which maintained the hydrostatic pressure. The upstream and downstream boundaries were placed at 3.5 and 2.5 ship lengths in the respective direction from the global coordinate system, resulting in 2.5 ship lengths clearance from each perpendicular. The computational domain and assigned boundary conditions are depicted in Figure 1.

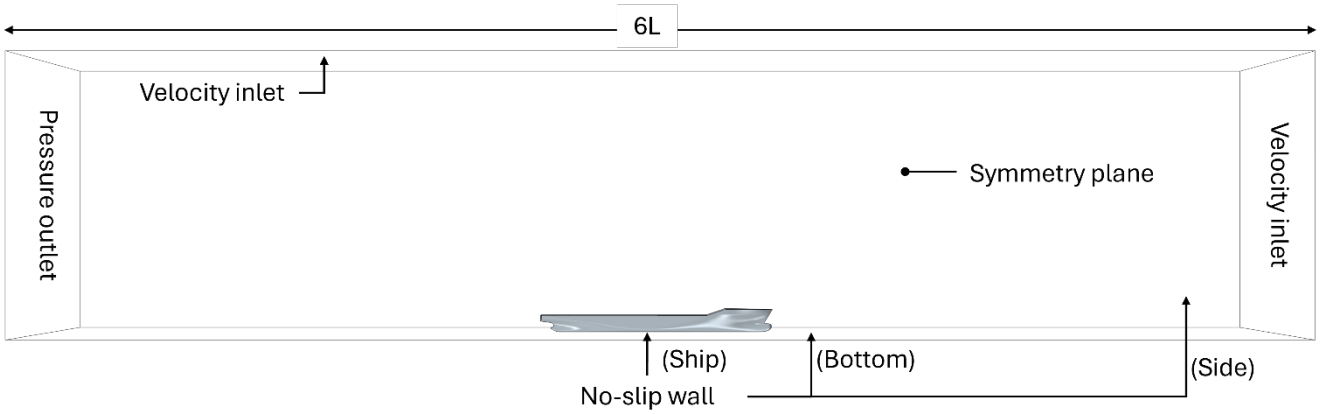

Figure 1. Computational domain and boundary conditions.

3.2 COMPUTATATIONAL MESH

The computational mesh was generated within the automatic facilities of Star-CCM+, consisting of flow-aligned hexahedral cells. A series of concentric refinements were created in the Kelvin wedge region in addition to a rectangular box encompassing the water surface in the entire computational domain where high-aspect ratio cells were created to capture deformations.

3.2 (a) Near-wall modelling approach

Near-wall modelling of turbulent flows is of critical importance to ensure the forces and moments acting on the vessel are accurately solved for. The approach laid out in (Terziev et al., 2022) was used to set the y^+ value to approximately 50 for the basis condition. The resulting near-wall mesh was copied to all conditions, which resulted in a y^+ of approximately 33 in the lowest speed case. The procedure for setting the y^+ *a priori* begins by approximating the ship's boundary layer as that of a flat plate with the same Reynolds number ($\delta = 0.382L/Re^{1/5}$, where δ is the boundary layer thickness and Re is the Reynolds number) and discretising the first 20% of the boundary layer where the majority of the flow velocity gradient is concentrated. The target y^+ = 50 is used in conjunction with the fluid density, ρ = 997.561 kg/m^3 and dynamic viscosity μ = 8.8875×10^{-4} Pa-s to estimate the thickness of the first cell layer ($2dy$) as shown in Eq. (1):

$$dy = y^+\nu/\sqrt{\tau_w/\rho} \quad (1)$$

Where τ_w is the shear wall stress, predicted using the ITTC correlation line and $\nu = \mu/\rho$. The number of layers (n) to be distributed over the discretised distance can be expressed through a geometric progression with a common ratio S=1.2 as shown in Eq. (2):

$$n = \log[1 - \delta(1 - S)/2dy]\ /\log\ (S) \quad (2)$$

A top view of the computational mesh is depicted in Figure 2, while the total number of cells was approximately 1.5 million cells with a small change in the number of cells depending on the water depth.

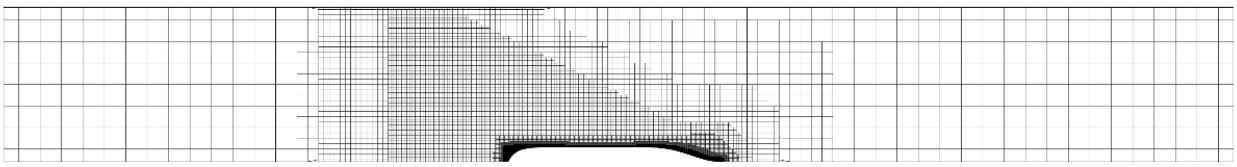

Figure 2. Computational mesh: top view of a slice through the mean water surface

3.3 MODELLING OF SHIP SQUAT

The account for the motion of the ship as a result of the hydrodynamic interaction between it and the bathymetry, a morphing mesh was utilised. This approach deforms the computational mesh to allow for 2-degrees of motion in the present case, namely, rotation around the y-axis (trim) and motion in the z-direction (sinkage). To prevent excessive mesh deformation and potential problems with stability of the solution, motion was initiated at least 5 seconds after the impulsive start of the simulation with hydrodynamic forces applied gradually following a further 10 seconds of simulation time. All simulations were allowed to run for a minimum of 150 seconds which also allowed the residuals to stabilise with a reduction of at least 3 orders of magnitude. In all cases, a combination of these criteria was used to judge convergence of the solution.

4 OPTIMISATION PROCEDURE

The optimisation procedure is based on the work of (Iqbal et al., 2025). The centre of gravity (CoG) optimisation technique to minimise squat and total resistance in fully confined water was conducted using a systematic approach that combines the response surface method (RSM) and a multi-objective genetic algorithm. The two key design variables in altering the CoG were the longitudinal centre of gravity (LCG) and the vertical centre of gravity (KG) of the ship. These variables significantly influence the ship's hydrodynamic performance, particularly squat and resistance, and were bounded within the range of −2.5 to 2.5 as codes. The conversion from codes to actual value is shown in Table 3, where -1, 0, and 1 indicate the minimum, initial, and maximum variation of design variables. The range between initial to maximum and minimum for LCG is ±2.5% and the KG is ±5%.

Table 3. Codification of design variables

Code	-1.414	-1	0	1	1.414
LCG	1.434	1.450	1.487	1.524	1.540
KG (0.75KM)	0.138	0.142	0.149	0.156	0.160

The two objective functions targeted for minimisation were squat and total resistance. To model the relationship between the design variables and the objective functions, a Central Composite Design (CCD) for two variables was employed, resulting nine combinations of load cases of two variables, including the initial condition. The nine combinations are shown in Table 4. The responses generated by this experimental design efficiently captures the nonlinear interactions between the variables while minimising the number of required simulations or experiments.

Table 4. Sample data generated from central composite design for two variables

No	Load Cases	x_1 code	x_2 code	LCG (m)	KG (m)
1	Initial	0	0	1.487	0.149
2	LC 1	1	1	1.524	0.156
3	LC 2	1	-1	1.524	0.142
4	LC 3	-1	1	1.450	0.156
5	LC 4	-1	-1	1.450	0.142
6	LC 5	-1.414	0	1.434	0.149
7	LC 6	1.414	0	1.540	0.149
8	LC 7	0	-1.414	1.487	0.138
9	LC 8	0	1.414	1.487	0.160

The results of the CCD procedure is a polynomial regression model which was developed for each objective function, squat and resistance. The general form of the regression model is shown in Eq. (3), where x_1 represents the LCG, $x_2$represents KG, and the coefficients a, b, c, d, e, f were determined from the CCD results after conducting the regression analysis. Then, these regression models formed the mathematical basis for optimisation

$$F(x_1, x_2) = a + bx_1 + cx_2 + d{x_1}^2 + e{x_2}^2 + f{x_1}^2{x_2}^2 \quad (3)$$

Where x_1 has a boundary condition of ±2.5% and x_2 a boundary condition of ±5%. To address the trade-off between minimising squat and resistance, a multi-objective genetic algorithm was applied. The algorithm began by generating an initial population of 500 solutions. Through iterative processes involving intermediate crossover and mutation, the algorithm explored the design space to produce new solutions. The fitness of each solution was evaluated using the polynomial regression models for squat and resistance, and non-dominated solutions were identified to construct a Pareto front. The optimisation process continued for 500 generations or until a maximum stall generation of 500 was reached, with tolerances set for function and constraint violations to ensure robust convergence.

The result of this process was a Pareto front representing the optimal trade-offs between squat and total resistance. Each point on the Pareto front corresponded to a solution where neither squat nor resistance could be improved without adversely affecting the other. These solutions were visualised in a Pareto plot, with squat and resistance represented on the x-axis and y-axis, respectively. The Pareto front provides insights into the relationship between the design variables and the objective functions, enabling decision-makers to select an optimal configuration of LCG and KG based on specific performance priorities. This approach effectively integrates RSM for efficient modelling and multi-objective genetic algorithm for robust multi-objective optimisation, offering a comprehensive framework for optimising ship performance in fully confined waters.

5 RESULTS AND DISCUSSION

5.1 VALIDATION AND VERIFICATION

The validation and verification process follows the norms set out by the ITTC (2008). Namely, the Grid Convergence Index procedure (Roache, 1997) was used to estimate the discretisation uncertainty. The numerical uncertainty is assumed to equal the discretisation uncertainty since iterative errors are negligible as explained in section 3.3. To obtain the discretisation uncertainty, a so-called grid triplet is required, which is obtained through a systematic change in the discretisation interval. The approach taken herein to satisfy the conditions of Richardson Extrapolation regarding cell aspect ratio and Courant number across the grid triplet is to magnify the spatial and temporal interval simultaneously (Salas, 2006). Then, the result from the Grid Convergence Index exercise is to obtain the spatio-temporal discretisation uncertainty, which begins with the definition of the convergence ratio (R) and observed order of accuracy (p):

$$R = \varepsilon_{32}/\varepsilon_{21} \quad (4)$$

$$p = \log(\varepsilon_{21}/\varepsilon_{32})\,/\log(r) \quad (5)$$

Where ε_{32} and ε_{21} are the difference between the coarse and medium, and medium and fine solution, respectively, while r is the refinement factor, chosen as $\sqrt{2}$, following ITTC (2008) and American Society of Mechanical Engineers (2009) guidelines. Once the observed order of accuracy is known, the uncertainty (U_N) follows:

$$U = 1.25\varepsilon_{21}/(r^p - 1) \quad (6)$$

Where the factor 1.25 is known as the factor of safety, used to increase the error's confidence interval from 50% to 95% and may be used when p is calculated using three solutions. A solution can be said to be validated if the error relative to the experiment is less than the validation uncertainty, defined as shown in Eq. (7). The results of the uncertainty estimation exercise and validation are shown in Table 4.

$$U_V = \sqrt{U_N^2 + U_E^2} \quad (7)$$

Where U_E is the experimental uncertainty. The experimental uncertainty in the present case was reported as 2.2% for resistance, and while the trim and sinkage show large uncertainties of approximately 90% at the low speed examined herein (Elsherbiny et al., 2019). To enable some measure of quality in sinkage and trim, the high-speed values of 3.47% and 4.64% are used, respectively.

Table 5. Discretisation uncertainty and validation exercise.

Parameter	Sinkage	Trim	Total resistance
Experimental value	2.09mm	0.022°	1.301N
Fine solution	2.03mm	0.009°	1.278N
Medium solution	2.05mm	0.001°	1.294N
Coarse solution	2.09mm	0.012°	1.317N
Convergence ratio	0.705	0.590	0.443
Observed order of accuracy	2.350	1.52	1.010
Discretisation uncertainty	0.794%	13.752%	3.825%
Experimental uncertainty	3.47% | 90%	4.64% | 90%	2.2%
Validation uncertainty	3.560% | 90.004%	14.514% | 91.045%	4.412%
Error (Fine – Experiment)	2.65%	60.02%	1.79%
Validated?	Yes | Yes	No | Yes	Yes

Table 5 shows that the solution is validated in sinkage regardless of whether the experimental uncertainty is taken as the low of high value reported by Elsherbiny et al. (2020) because the error relative to the experimental value is 2.65%. In the case of resistance, the experimental error is also sufficiently small to allow a successful validation. Although the disagreement in trim value is small, the relative percentage difference is significant, meaning that only the high level of experimental uncertainty permits the validation to be successful. An important aspect of the discretisation uncertainty estimate is to ensure the observed orders of accuracy are close to or not significantly higher than the theoretical value of $p = 2$. The results reported in Table 5 show that the order of accuracy predicted for sinkage is close to the theoretical value, while trim and total resistance exhibit smaller values, which are known to magnify the uncertainty. These properties of the approach to the asymptotic range give confidence in the robustness of the solution.

5.2 SINKAGE, TRIM AND RESISTANCE COEFFICIENTS

Presentation of the results from the systematic variation in position of the LCG proceeds with a description of the obtained values. To facilitate interpretation of the data, the results are presented by showing the property of interest, such as sinkage in the case of Figure 3, against relative changes in the position of the LCG while changes in the position of the KG are included via variations in the colour.

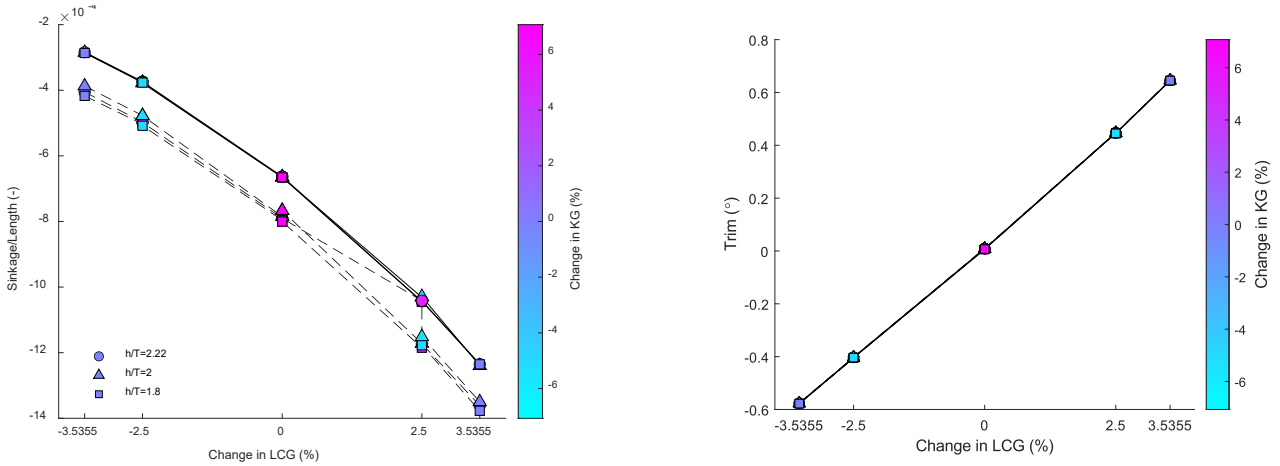

Figure 3. Sinkage and trim values obtained for all case studies. Solid lines show w/L = 1.5, while dashed lines show w/L = 1.

Figure 3 shows that sinkage is affected weakly by the position of the KG. All points except when the LCG is moved forward by 2.5% show that the sinkage change between case studies, for example the difference between h/T=2.2, h/T=2, and h/T=1.8 are within 1.5%. The aforementioned variation is within the uncertainty band reported in section 5.1. Thus, the variation with KG could be explained by the limitations of the computational model. Nevertheless, the results demonstrate that LCG has a significant effect on sinkage, which may increase by a factor of 7 across the examined case studies. Similarly, the trim is dominated by changes in the position of the LCG and shows negligible dependence on the KG. These results can be explained by the low value of the depth Froude number. At such speeds, the hydrodynamic moment generating trim is small, hence, the results are dominated by the initial trim.

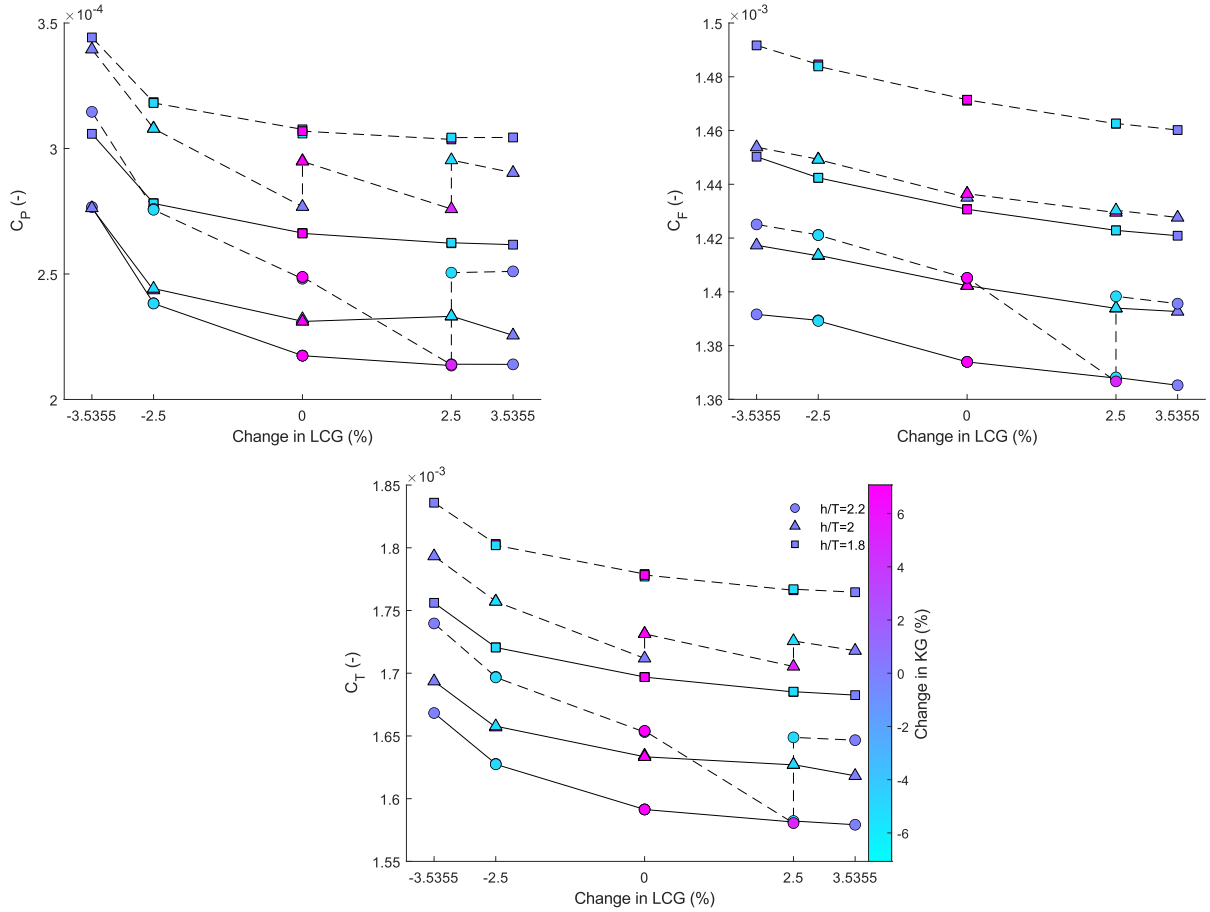

Figure 4. Pressure, Frictional, and total resistance coefficient values obtained for all case studies. Solid lines show w/L=1.5 and dashed lines show w/L=1.

Unlike sinkage and trim, the total resistance exhibits a more complex pattern owing to the change in width and depth of the waterway. When the dimensionless width of the waterway corresponds to w/L=1.5, the influence of KG is limited, as evidenced by the smooth curved described by the total resistance coefficient values in those cases across the range of LCG values. However, when the dimensionless width is reduced, the KG shows an influence on the results driven by apparent

changes in sinkage rather than trim. Figure 3 and Figure 4 jointly show that the variations in KG are responsible for the changes in the resistance. Unlike potential flow models which are not able to model the frictional component change, the computational model captures these and shows that the spike in resistance at ΔLCG=2.5% with variations in KG occurs not solely due to pressure resistance or its component, the wave resistance, which is typically isolated and optimised for. Instead, the frictional resistance and the pressure resistance show a similar pattern, particularly for the deepest case (h/T=2.2). With decreases in water depth, hydrodynamic forces and moments increase, and hence, the influence of variations in KG appears to decrease so that when h/T=1.8, the resistance curve versus LCG becomes smooth and shows no influence on the KG.

5.3 PARETO FRONTS

As described previously, the systematic variations in the LCG and KG were used to construct a mathematical model which is fed into a multi-objective genetic optimisation model with the purpose of defining the set of optimum solutions. This set of optima, known as the Pareto front, can be used to establish the trade-off in optimum arrangement directly through parameters of interest. For the purposes of this paper, the total resistance coefficient and squat, defined as the maximum vertical deviation of the ship, taking into account the sinkage and trim, was used. It should be noted that unlike sinkage, squat is defined positive downwards to facilitate the minimisation process of the multi-objective optimiser. The results, separated for w/L=1.5 and w/L=1 are shown in Figure 5.

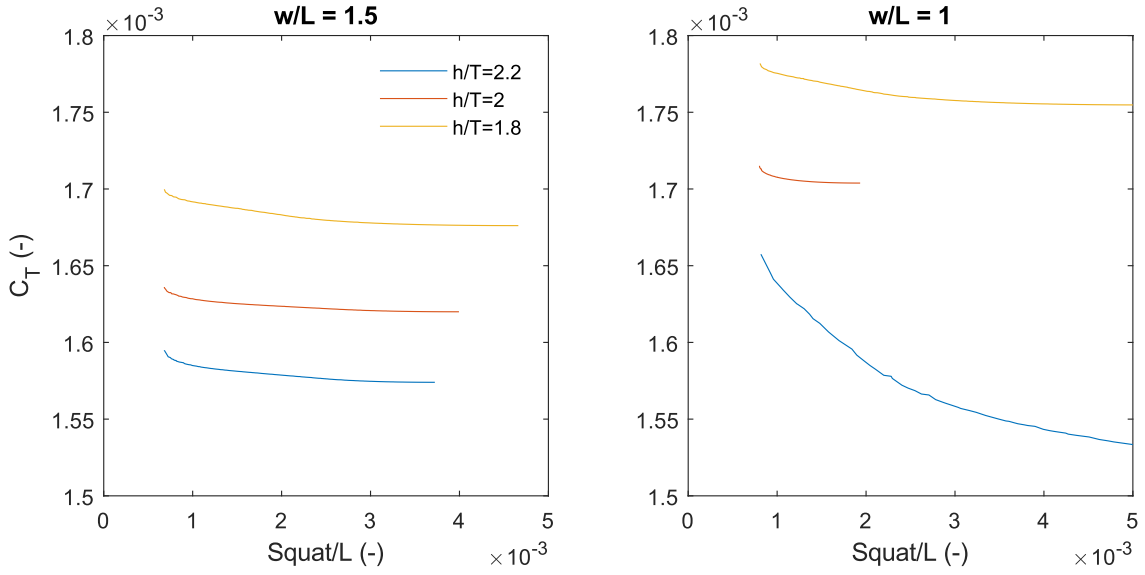

Figure 5. Pareto fronts of the total resistance coefficient and dimensionless squat for w/L=1.5 and w/L=1.

Figure 5 shows that despite the identical value in the depth Froude number across the case studies, there are significant variations in the set of possible optima. Specifically, the h/T=1.8 case is always characterised by a higher total resistance coefficient by no less than approximately 6.5% and 3.4% relative to h/T=2.2 and h/T=2, respectively, for the same dimensionless squat values at w/L=1.5. Similarly, the maximum differences in this case are 6.75% and 3.93%. Reducing the channel width causes a shift of the maximum disagreement magnifying the difference to up to 16.65% and 3.9%. More importantly, a consequence of the pareto fronts shown in Figure 5 is that an increase in squat can be linked to a reduction in resistance – a trend preserved across all case studies in varying degrees. Generally, a lower squat was associated with a trim by stern, hence, the results can be interpreted by the fact that the vessel ought to have a small trim by bow to reduce resistance; a result previously observed for the KCS by Campbell et al. (2022).

6 CONCLUSIONS AND FUTURE WORK

The effect of variation in the position of centre of gravity on ship hydrodynamics in fully confined water were examined using Computational Fluid Dynamics based on the Reynolds Averaged-Navier Stokes approach. Results were validated for a depth Froude number of 0.303 and a sample channel geometry against experimental results. Then, six channel geometries and nine systematically varied centre of gravity positions within the range ±2.5% horizontally and ±5% vertically were modelled for a depth Froude number of 0.303.

The obtained results show that trim is influenced weakly by the hydrodynamic moment generated due to forward motion, allowing the initial trim due to the change in centre of gravity to dominate the response. While the main response in sinkage was also dominated by the initial trim, it was found that the highest position of the centre of gravity resulted in a change in

sinkage which caused a spike in resistance coefficients. Interestingly, the pressure and shear force coefficients acting on the hull were affected causing in the same trend, hence, the effect on the total resistance coefficient was significant.
A complex interaction is revealed that depends on the vertical and horizontal position of the centre of gravity. Specifically, it is shown that sinkage is affected weakly by variations of the centre of gravity in the vertical direction, which were predicted to be around 1.5%, a value that lies within the discretisation uncertainty band. Conversely, variations in the LCG may alter the sinkage by a factor of 7. Resistance coefficients curves show spikes, only explainable through changes in the vertical position of the centre of gravity. For example, C_T may change by approximately 4% solely due to variations in VCG in a given case study. It is also revealed that such changes due to the position of vertical position of the entre of gravity become apparent only when the waterway width is small or equivalently, when the blockage is high.
The results obtained from systematically varying the centre of gravity were fed to a multi-objective genetic algorithm after a response surface model of the data was constructed. The multi-objective optimisation algorithm was used to construct Pareto fronts describing the trade-off between squat, the maximum reduction in underkeel clearance, and the total resistance coefficient which showed that a small squat is linked to elevated resistance. This was interpreted through the lens of the direction of trim since it is known that a small trim by bow contributes to energy efficiency of the target ship.
There are several ways in which the present study may be extended, ranging from the incorporation of other velocities to changes in blockage and self-propulsion. The former two are of particular interest since the depth Froude number was preserved for all case studies in the present paper rather than maintaining the velocity. It is interesting to observe how changes such as the speed and further reductions in the channel width may impact the results, particularly in cases where the hydrodynamic moment may cause trim of similar magnitude to the initial trim.

7 ACKNOWLEDGEMENTS

Results were obtained using the ARCHIE-WeSt High Performance Computer (www.archie-west.ac.uk) based at the University of Strathclyde.

8 REFERENCES

ASME (American Society of Mechanical Engineers). (2009). Standard for Verification and Validation in Computational Fluid Dynamics and Heat Transfer - ASME V&V 20-2009. In *ASME International*.

Barrass, C. B., & Derrett, D. R. (2012). Chapter 42 – Ship Squat in Open Water and in Confined Channels. *Ship Stability for Masters and Mates*, 367–388. https://doi.org/10.1016/B978-0-08-097093-6.00042-6

Campbell, R., Terziev, M., Tezdogan, T., & Incecik, A. (2022). Computational fluid dynamics predictions of draught and trim variations on ship resistance in confined waters. *Applied Ocean Research*, *126*(August), 103301. https://doi.org/10.1016/j.apor.2022.103301

Chillcce, G., & Moctar, O. (2022). Viscous effects on squat. *Applied Ocean Research*, *125*(July), 103252. https://doi.org/10.1016/j.apor.2022.103252

Cisek, J. M. (2025). Weather-driven variations in optimum trim of a refrigerated cargo carrier: insights from ocean crossing voyage. *Journal of Ocean Engineering and Marine Energy*. https://doi.org/10.1007/s40722-024-00378-2

Elsherbiny, K., Terziev, M., Tezdogan, T., Incecik, A., & Kotb, M. (2020). Numerical and experimental study on hydrodynamic performance of ships advancing through different canals. *Ocean Engineering*, *195*(106696). https://doi.org/10.1016/j.oceaneng.2019.106696

Elsherbiny, K., Tezdogan, T., Kotb, M., Incecik, A., & Day, S. (2019). Experimental analysis of the squat of ships advancing through the New Suez Canal. *Ocean Engineering*, *178*(November 2018), 331–344. https://doi.org/10.1016/j.oceaneng.2019.02.078

EMSA (European Maritime Safety Agency). (2023). *Annual Overview of Marine Casualties and Incidents*.

Härting, A., Laupichler, A., & Reinking, J. (2009). Considerations on the squat of unevenly trimmed ships. *Ocean Engineering*, *36*(2), 193–201. https://doi.org/10.1016/j.oceaneng.2008.10.003

Hirt, C. W. W., & Nichols, B. D. D. (1981). Volume of fluid (VOF) method for the dynamics of free boundaries. *Journal of Computational Physics*, *39*(1), 201–225. https://doi.org/10.1016/0021-9991(81)90145-5

Iqbal, M., Terziev, M., Tezdogan, T., & Incecik, A. (2025). Hull form optimisation to minimise the total resistance and dynamic responses of small fishing vessels. *Ocean Engineering*, *321*, 120357. https://doi.org/10.1016/j.oceaneng.2025.120357

ITTC. (2008). Uncertainty Analysis in CFD Verification and Validation Methodology and Procedures. *25th ITTC 2008, Resistance Committee*, 12. http://ittc.info/media/4184/75-03-01-01.pdf

Korkmaz, K. B., Werner, S., & Bensow, R. (2023). Investigations on experimental and computational trim optimisation methods. *Ocean Engineering*, *288*. https://doi.org/10.1016/j.oceaneng.2023.116098

Le Strat, M., & Terziev, M. (2025). Scale effects on ship vertical force and trim moment in calm water. *Physics of Fluids*, *37*(1). https://doi.org/10.1063/5.0243505

Panagiotakopoulos, T., Filippopoulos, I., Filippopoulos, C., Filippopoulos, E., Lajic, Z., Violaris, A., Panagiotis Chytas, S., & Kiouvrekis, Y. (2022, July 18). Vessel's trim optimization using IoT data and machine learning models. *13th International Conference on Information, Intelligence, Systems & Applications (IISA)*. https://marantankers.gr/

Roache, P. J. (1997). Quantification of Uncertainty in Computational Fluid Dynamics. *Annual Review of Fluid Mechanics*, *29*(1), 123–160. https://doi.org/10.1146/annurev.fluid.29.1.123

Salas, M. D. (2006). Some observations on grid convergence. *Computers and Fluids*, *35*(7), 688–692. https://doi.org/10.1016/j.compfluid.2006.01.003

Terziev, M., Tezdogan, T., & Incecik, A. (2019). Application of eddy-viscosity turbulence models to problems in ship hydrodynamics. *Ships and Offshore Structures*, 1–24. https://doi.org/10.1080/17445302.2019.1661625

Terziev, M., Tezdogan, T., & Incecik, A. (2022). Scale effects and full-scale ship hydrodynamics: A review. *Ocean Engineering*, *245*(November 2021), 110496. https://doi.org/10.1016/j.oceaneng.2021.110496

Terziev, M., Tezdogan, T., Oguz, E., Gourlay, T., Demirel, Y. K., & Incecik, A. (2018). Numerical investigation of the behaviour and performance of ships advancing through restricted shallow waters. *Journal of Fluids and Structures*, *76*, 185–215. https://doi.org/10.1016/j.jfluidstructs.2017.10.003

Tu, H., Xia, K., Zhao, E., Mu, L., & Sun, J. (2023). Optimum trim prediction for container ships based on machine learning. *Ocean Engineering*, *277*. https://doi.org/10.1016/j.oceaneng.2022.111322

9 AUTHORS BIOGRAPHY

Brief biographies are required for all authors e.g.:

Momchil Terziev is assistant professor in naval architecture at the Department of Naval Architecture, Ocean and Marine Engineering at the University of Strathclyde. His research interests lie in scale effects and shallow water ship hydrodynamics.
Muhammad Iqbal is assistant professor at Diponegoro University within the Faculty of Engineering. His research interests include modelling and performance of small fishing boats.
Yujia Wei is research fellow in fellow in multiphysics modelling at the University of Cranfield. His research interests include computational modelling of hydroelasticity of marine structures and AI applications in the maritime field.
Atilla Incecik is professor of offshore engineering at the Department of Naval Architecture, Ocean and Marine Engineering at the University of Strathclyde. His research interests span ocean and marine engineering with applications to ships and offshore structures.